Available online at www.sciencedirect.com

ScienceDirect

Journal of the Nigerian Mathematical Society 35 (2016) 1–17

Journal of the Nigerian Mathematical Society

www.elsevier.com/locate/jnnms

Casson fluid flow with variable thermo-physical property along exponentially stretching sheet with suction and exponentially decaying internal heat generation using the homotopy analysis method

I.L. Animasaun*, E.A. Adebile, A.I. Fagbade

Department of Mathematical Sciences, Federal University of Technology Akure, Ondo State, Nigeria

Received 12 July 2014; received in revised form 27 September 2014; accepted 17 January 2015
Available online 23 February 2015

Abstract

This article studies the motion of temperature dependent plastic dynamic viscosity and thermal conductivity of steady incompressible laminar free convective magnetohydrodynamic (MHD) Casson fluid flow over an exponentially stretching surface with suction and exponentially decaying internal heat generation. It is assumed that the natural convection is driven by buoyancy and space dependent heat generation. The viscosity and thermal conductivity of Casson fluid is assumed to vary as a linear function of temperature. By using suitable transformation, the governing partial differential equations corresponding to the momentum and energy equations are converted into non-linear coupled ordinary differential equations and solved by the Homotopy analysis method. A new kind of averaged residual error is adopted and used to find the optimal convergence control parameter. A parametric study is performed to illustrate the influence of Prandtl number, Casson parameter, temperature dependent viscosity, temperature dependent thermal conductivity, Magnetic parameter and heat source parameter on the fluid velocity and temperature profiles within the boundary layer. The flow controlling parameters are found to have a profound effect on the resulting flow profiles.

Keywords: Casson fluid; Variable viscosity; Variable thermal conductivity; Boundary value problem; Homotopy analysis method

1. Introduction

As fluid flows on continuous moving surface, boundary layer is formed and it's of important in nature due to its influence on the transport phenomena. Natural convection arises within the fluid when temperature changes cause density variation leading to buoyancy forces which act directly on the fluid elements. Theoretical and experimental study on heat transfer MHD free convection flow with thermal radiation effects on a vertical plate has received

Peer review under responsibility of Nigerian Mathematical Society.
* Corresponding author.
E-mail addresses: anizakph2007@gmail.com (I.L. Animasaun), eaadebiletri@gmail.com (E.A. Adebile), yemi2favours@yahoo.co.uk (A.I. Fagbade).

http://dx.doi.org/10.1016/j.jnnms.2015.02.001

deep interest during the last decades. The study of magnetohydrodynamics flow and heat transfer over a continuous stretching sheet is one of the very important problems in fluid dynamics due to its numerous applications in industrial manufacturing processes such as paper production, manufacturing of ceramic polymer extrusion and production of plastic. Sakiadis [1,2] started a research on boundary layer behavior when fluid flows on a continuous solid surface. Crane [3] furthered the research and considered the boundary layer flow caused by a stretching sheet which moves with a velocity varying linearly with the distance from a fixed point. Carragher and Crane [4] continued this research and studied heat transfer aspect under the conditions when the temperature difference between the surface and the ambient fluid is proportional to a power of the distance from a fixed point. Ibrahim [5] adopted numerical analysis method in order to study heat and mass transfer effects on steady two dimensional flow of a viscous incompressible, electrically conducting dissipating fluid past an exponentially stretching surface in the presence of magnetic field, heat generation and radiation. In the governing equation, the author considered magnetic field term and square of velocity component in x-direction. Miansari et al. [6] applied the Homotopy analysis method together with Pade-Approximation to solve dimensionless momentum and energy equations considering the case of a two dimensional incompressible flow passing over a wedge. They also presented efficiency of HAM together with trial and error method for solving the momentum equation. They also solved the momentum equation by considering the Pade-Approximation with HAM. The flow and heat transfer over an exponentially stretching surface have been studied by many researchers. Elbashbeshy [7] investigated wall mass suction, Khan and Sanjayanand [8] presented the boundary layer flow of viscoelastic fluid and heat transfer over an exponentially stretching sheet with viscous dissipation effect, Partha et al. [9] reported a similarity solution for mixed convection flow past an exponentially stretching surface. Ishak [10] studied the magnetohydrodynamic (MHD) boundary layer flow over an exponentially shrinking sheet in the presence of thermal radiation, Bhattacharyya [11] discussed the boundary layer flow and heat transfer caused due to an exponentially shrinking sheet and Bhattacharyya and Pop [12] showed the effect of external magnetic field on the flow over an exponentially shrinking sheet. Recently, Bhattacharyya and Vajravelu [13] described the stagnation point boundary layer flow due to exponentially shrinking sheet for Newtonian fluid.

The study of non-Newtonian fluids has attracted much attention because of their extensive variety of applications in engineering and industry especially in extraction of crude oil from petroleum products, production of plastic materials and syrup drugs. In the category of non-Newtonian fluids, Casson fluid has distinct features. Casson fluid is one of the types of such non-Newtonian fluids, which behaves like an elastic solid, and for this kind of fluid, a yield shear stress exists in the constitutive equation. Non-Newtonian transport phenomena arise in many branches of mechanical and chemical engineering and also in food processing. Some materials e.g. muds, condensed milk, glues, printing ink, emulsions, paints, sugar solutions, shampoos and tomato pastes exhibit almost all the properties of non-Newtonian fluid. This rheological model was introduced originally by Casson [14] in his research on a flow equation for pigment oil-suspensions of printing ink. Casson model constitutes a plastic fluid model which exhibits shear thinning characteristics, yield stress, and high shear viscosity. According to a research conducted by Rao et al. [15], it is stated that Casson fluid model is reduced to a Newtonian fluid at a very high wall shear stress, i.e., when the wall stress is much greater than yield stress. This fluid model also approximates reasonably well the rheological behavior of other liquids including physiological suspensions, foams, cosmetics, syrups, etc. Although different models are proposed to explain the behavior of non-Newtonian fluids, the most important non-Newtonian fluid possessing a yield value is the Casson fluid. Bird et al. [16] investigated the rheology and flow of visco-plastic materials and reported that the Casson model constitutes a plastic fluid model which exhibits shear thinning characteristics, yield stress, and high shear viscosity. In 2007, Evan Mitsoulis discussed in detail on the stress-deformation behavior of viscoplastic models (i.e. Bingham models, Herschel–Bulkley model and the Casson model) and different constitutive equations proposed in [16]. Mitsoulis [17] further reviews several benchmark problems of viscoplastic flows, such as entry and exit flows from dies, flows around a sphere and a cylinder and squeeze flows. The fundamental analysis of the flow field of non-Newtonian fluids in a boundary layer adjacent to a stretching sheet or an extended surface is very important and is an essential part in the study of fluid dynamics and heat transfer [18]. Hayat et al. [19] investigated Soret and Dufour effects on magnetohydrodynamic (MHD) flow of Casson fluid. Fredrickson [20] investigated the steady flow of a Casson fluid in a tube. The unsteady boundary layer flow and heat transfer of a Casson fluid over a moving flat plate with a parallel free stream were studied by Mustafa et al. [21] and they solved the problem analytically using the Homotopy analysis method (HAM). Recently, Animasaun [22] presented the effects of some thermo-physical parameters on non-darcian MHD dissipative Casson fluid flow along linearly stretching vertical surface when there exists migration of colloidal particles in response to a macroscopic temperature.

Internal energy generation can be explained as a scientific method of generating heat within a body by a chemical, electrical or nuclear process. Natural convection induced by internal heat generation is a common phenomenon in nature. Examples include motion in the atmosphere where heat is generated by absorption of sunlight [see Tasaka et al. [23]]. In the energy equation, Sahin [24] considered heat generation rate resulting from the radiation absorption by differentiating the radiation intensity. Crepeau and Clarksean [25] carried out a similarity solution for a fluid with an exponentially decaying heat generation term and a constant temperature vertical plate under the assumption that the fluid has an internal volumetric heat generation. An exponential form is used for the internal energy generation term. In many situations, there may be appreciable temperature difference between the surface and the ambient fluid. This necessitates the consideration of temperature dependent heat sources that may exert a strong influence on the heat transfer characteristics [26]. The study of heat generation or absorption effects is important in view of several physical problems such as fluids undergoing exothermic or endothermic chemical reaction; although, exact modeling of internal heat generation or absorption is quite difficult, some simple mathematical models can express its average behavior for most physical situations [27]. Recently, Makinde [28] analyzed the effect of variable viscosity on thermal boundary layer over a permeable flat plate with radiation and a convective surface boundary condition. The purpose of this theoretical study is to unravel the behavior of velocity and temperature profiles of Casson flow with variable plastic dynamic viscosity and thermal conductivity within boundary layer over a vertical surface with suction and space dependent internal heat generation by using analytical approximate method of solution. The governing partial differential equations are modified and converted to nonlinear ordinary differential equations using suitable similarity transformations. The transformed self-seminar ODE's are solved by the Homotopy analysis method.

2. Mathematical formulation

A steady two-dimensional laminar free convective boundary layer flow of a viscous incompressible electrically conducting fluid flow along a vertical exponentially stretching sheet in the presence of suction is considered for a theoretical study. The surface is elastic. The motion of an incompressible non Newtonian fluid is induced because of the stretching property of the surface, buoyancy effects which are generated by gradients in the temperature field of a dissolved species and space dependent internal heat generation. This occurs in view of the elastic properties of the surface parallel to the x-axis through equal and opposite forces when the origin is fixed at $x = y = 0$. The physical model is shown in Fig. 1. A magnetic field B_o of uniform strength is applied transversely to the direction

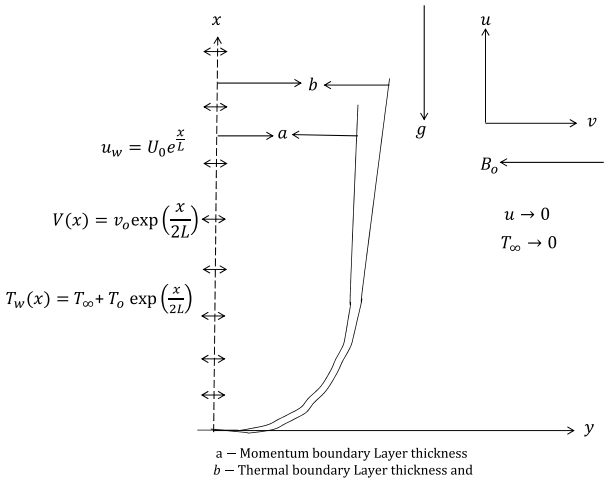

Fig. 1. Flow configuration and the coordinate system.

of the flow. Since the fluid pressure is constant throughout the boundary, it is assumed that induced magnetic field is small in comparison to the applied magnetic field; hence it is neglected. Under the above assumptions and invoking the Boussinesq approximation, the boundary layer equations governing the flow and heat transfer of a viscous and

incompressible fluid can be written as

$$\frac{\partial u}{\partial x}+\frac{\partial v}{\partial y}=0, \tag{1}$$

$$u\frac{\partial u}{\partial x}+v\frac{\partial u}{\partial y}=\vartheta\frac{\partial^2 u}{\partial y^2}-\frac{\sigma B^2}{\rho}u+g\beta^{+}(T-T_\infty), \tag{2}$$

$$u\frac{\partial T}{\partial x}+v\frac{\partial T}{\partial y}=\frac{\kappa}{\rho Cp}\frac{\partial^2 T}{\partial y^2}-\frac{1}{\rho Cp}\frac{\partial q_r}{\partial y}+\frac{Q_o(T_w-T_\infty)}{\rho Cp}exp\left(-ny\sqrt{\frac{U_o}{2\vartheta L}}exp\left(\frac{x}{2L}\right)\right) \tag{3}$$

where T is the temperature of the fluid, $\vartheta=\frac{\mu}{\rho}$ is the kinematic coefficient of viscosity with μ being the fluid viscosity and ρ is the fluid density, $\alpha=\frac{\kappa}{\rho Cp}$ is the thermal diffusivity with κ being the fluid thermal conductivity and Cp is the heat capacity at constant pressure. The dimensionless space internal heat generation term in energy equation is modeled following the concept introduced in [29–31] where Q_o is the coefficient of space-dependent internal heat generation. From the definition of viscosity ($\tau=\mu\frac{\partial u}{\partial y}|_{y=0}$) and according to [18,20] it is assumed that the rheological equation of an isotropic and incompressible flow of a Casson fluid can be written as

$$\begin{aligned}\tau_{ij}&=\left(\mu_b+\frac{P_y}{\sqrt{2\pi}}\right)2e_{ij}\quad \text{when } \pi>\pi_c,\\ \tau_{ij}&=\left(\mu_b+\frac{P_y}{\sqrt{2\pi_c}}\right)2e_{ij}\quad \text{when } \pi<\pi_c,\end{aligned} \tag{4}$$

P_y is known as yield stress of the fluid, mathematically expressed as

$$P_y=\frac{\mu_b\sqrt{2\pi}}{\beta}, \tag{5}$$

μ_b is known as plastic dynamic viscosity of the non-Newtonian fluid, π is the product of the component of deformation rate with itself (i.e. $\pi=e_{ij}e_{ij}$), where e_{ij} is the (i,j)th component of the deformation rate and π_c is the critical value based on the non-Newtonian model. In a case of Casson fluid (Non Newtonian) flow, where $\pi>\pi_c$, it is possible to say that

$$\mu=\mu_b+\frac{P_y}{\sqrt{2\pi}}. \tag{6}$$

Substituting (5) into (6), the kinematics viscosity of Casson fluid is now depending on plastic dynamic viscosity μ_b, density ρ and Casson parameter β

$$\vartheta=\frac{\mu_b}{\rho}\left(1+\frac{1}{\beta}\right). \tag{7}$$

Rosseland approximation requires that the media is optically dense media and radiation travels only a short distance before being scattered or absorbed. Since we are considering a situation in which the radiation of heat within optically thick Casson fluid exists before the heat is scattered, radiative heat transfer is taken into account. Rosseland equation which is a simplified model of Radiative Transfer Equation (RTE) is adopted to account for this effect. When material has a great extinction coefficient, it can be treated as optically thick. q_r is the radiative heat flux and is defined using the Rosseland approximation [32], [33] as

$$q_r=\frac{-4\sigma}{3k^*}\frac{\partial T^4}{\partial y}, \tag{8}$$

where σ is the Stefan–Boltzmann constant and k^* is known as the absorption coefficient. Following [14,16,17], we assumed that the temperature differences within the flow are sufficiently small such that T^4 may be expressed as a linear function of the freestream temperature T_∞. This is obtained by expanding T^4 in a Taylor series about T_∞ and

neglecting higher order terms, we obtained

$$T^4 \approx T_\infty^4 + 4T_\infty^3 T - 4T_\infty^3 T_\infty, \tag{9}$$

$$\frac{\partial q_r}{\partial y} = \frac{\partial}{\partial y}\left(\frac{-4\sigma}{3k^*}\frac{\partial T^4}{\partial y}\right) = \frac{\partial}{\partial y}\left(\frac{-4\sigma}{3k^*}\frac{\partial T^4}{\partial T}\frac{\partial T}{\partial y}\right). \tag{10}$$

Upon substitution, we obtained

$$\frac{\partial q_r}{\partial y} = \frac{-16\sigma T_\infty^3}{3k^*}\frac{\partial^2 T}{\partial y^2}. \tag{11}$$

We are interested in the case where plastic dynamic viscosity μ_b and thermal conductivity of Casson fluid κ vary as a linear function of temperature. Molecules of fluids exert forces of attraction on each other either in motion or at rest. In liquids, this kind of force is strong enough to keep the mass together but not strong enough to keep it rigid like that of solid. When a fluid flows over a surface, the layer next to the surface may become attached to it (wets the surface "no slip condition"). Casson fluid exhibits shear thinning characteristics which can conduct heat when exposed. This assumption is valid since it is known that the physical properties of the fluid may change significantly with temperature. For lubricating fluids, heat generated by the internal friction and the corresponding rise in temperature affects the viscosity of the fluid and so the fluid viscosity can no longer be assumed constant. The increase of temperature leads to a local increase in the transport phenomena by reducing the viscosity across the momentum boundary layer and so the heat transfer rate at the wall is also affected greatly. In industrial systems, fluids can be subjected to extreme conditions such as high temperature, pressure, high shear rates and external heating (Ambient Temperature) and each of these factors can lead to high temperature being generated within the fluid. Modified governing equations are:

$$u\frac{\partial u}{\partial x} + v\frac{\partial u}{\partial y} = \frac{\mu_b(T)}{\rho}\left(1+\frac{1}{\beta}\right)\frac{\partial^2 u}{\partial y^2} + \frac{1}{\rho}\left(1+\frac{1}{\beta}\right)\frac{\partial u}{\partial y}\frac{\partial \mu_b(T)}{\partial T}\frac{\partial T}{\partial y} - \frac{\sigma B^2}{\rho}u + g\beta^+(T-T_\infty), \tag{12}$$

$$\begin{aligned} u\frac{\partial T}{\partial x} + v\frac{\partial T}{\partial y} \;=\; & \frac{\kappa(T)}{\rho Cp}\frac{\partial^2 T}{\partial y^2} + \frac{1}{\rho Cp}\frac{\partial T}{\partial y}\frac{\partial T}{\partial y}\frac{\partial \kappa(T)}{\partial y} + \frac{16\sigma T_\infty^3}{3k^*}\frac{\partial^2 T}{\partial y^2} \\ & + \frac{Q_o(T_w - T_\infty)}{\rho Cp} exp\left(-ny\sqrt{\frac{U_o}{2\vartheta L}} exp\left(\frac{x}{2L}\right)\right). \end{aligned} \tag{13}$$

In Physics, it is a well-known fact that, if an object is on an elastic surface at rest, when the surface is stretched; the object also tends to move towards the direction of the pull. The surface of the plate in Fig. 1 is assumed to be highly elastic and is stretched in the x-direction with a velocity $u = U_0 exp(\frac{x}{L})$. Eqs. (12) and (13) are subject to the following boundary conditions

$$u = U_0 exp\left(\frac{x}{L}\right), \qquad v = -v_o exp\left(\frac{x}{2L}\right), \qquad T = T_\infty + T_0 exp\left(\frac{x}{2L}\right) \quad \text{at } y = 0 \tag{14}$$

$$u \to 0, \qquad T \to T_\infty, \quad \text{as } y \to \infty. \tag{15}$$

In this research, U_0 is a constant and L is the reference length. It is very important to note that, the exponential velocity at the wall $U_0 exp\left(\frac{x}{L}\right)$ is valid only when $x \ll L$. When $x \geq L$, it is very obvious that the effect of the exponential property on wall velocity may skyrocket. Also, in the third term of (14), it is obvious that $(T_w - T_\infty) = T_0 exp\left(\frac{x}{2L}\right)$. The following relations are introduced for u and v as $u = \frac{\partial \psi}{\partial y}$ and $v = -\frac{\partial \psi}{\partial x}$ respectively. Here $\psi(x, y)$ is the stream function. Introduce similarity variables

$$\eta = y\sqrt{\frac{U_0}{2\vartheta L}} exp\left(\frac{x}{2L}\right), \qquad \psi(x, y) = \sqrt{2\vartheta L U_0} f(\eta) exp\left(\frac{x}{2L}\right),$$

dimensionless temperature, temperature dependent viscosity model in [34,35] and temperature dependent thermal conductivity model in [36,37] respectively as

$$\theta(\eta) = \frac{T - T_\infty}{T_w - T_\infty}, \qquad \mu_b(T) = \mu_b^*[a + b(T_w - T)], \qquad \kappa(T) = \kappa^*[1 + \delta(T - T_\infty)]. \tag{16}$$

These automatically satisfied continuity equation (1) and we obtained the following locally similar ordinary differential equations:

$$\left(1+\frac{1}{\beta}\right)[1+\xi-\theta\xi]\frac{d^3f}{d\eta^3}-\xi\left(1+\frac{1}{\beta}\right)\frac{d\theta}{d\eta}\frac{d^2f}{d\eta^2}-2\left(\frac{df}{d\eta}\right)^2+f\frac{d^2f}{d\eta^2}-H_a\frac{df}{d\eta}+J_T\theta\xi=0, \tag{17}$$

$$\left[1+\frac{4}{3N}+\theta\varepsilon\right]\frac{d^2\theta}{d\eta^2}+\varepsilon\left(\frac{d\theta}{d\eta}\right)^2-P_r\theta\frac{df}{d\eta}+P_rf\frac{d\theta}{d\eta}+P_r\gamma exp(-n\eta)=0. \tag{18}$$

Together with the boundary conditions

$$\frac{df}{d\eta}=1,\qquad f=S,\qquad \theta=1\quad \text{at } \eta=0 \tag{19}$$

$$\frac{df}{d\eta}\to 0,\qquad \theta\to 0,\quad \text{as } \eta\to\infty \tag{20}$$

where $\xi=b(T_w-T_\infty)$ is the variable plastic dynamic viscosity parameter, $\beta=\frac{\mu_b\sqrt{2\pi}}{P_y}$ is the non-Newtonian Casson parameter, $J_T=\frac{2g\beta^+L}{bU_0^2exp\left(\frac{2x}{L}\right)}$ is the local modified Grashof related parameter, $\varepsilon=\delta(T_w-T_\infty)$ is the variable thermal conductivity parameter, $P_r=\frac{C_p\mu}{\kappa}$ is the Prandtl number, $\gamma=\frac{Q_0}{\rho Cp}\frac{2L}{U_0exp\left(\frac{x}{L}\right)}$ is the space dependent internal heat source parameter, $H_a=\frac{2\sigma B_o^2L}{\rho U_o}$ is the magnetic field parameter and $N=\frac{\kappa\kappa^*}{4\sigma T_\infty^3}$ is the Radiation parameter. The suction parameter $S=\frac{v_o2L}{\sqrt{2\vartheta LU_o}}$ holds by invoking $\eta=0$. For practical applications, the major physical quantities of interest are the local skin friction coefficient and Nusselt number. The first physical quantities of interest is the wall skin friction coefficient C_f defined as

$$C_f=\frac{\tau_w}{\rho\left(U_0exp\left(\frac{x}{2L}\right)\right)^2}\quad \text{where } \tau_w=\left(\mu_b+\frac{P_y}{\sqrt{2\pi}}\right)\left.\frac{\partial u}{\partial y}\right|_{y=0}$$

τ_w is known as Shear stress or skin friction along the stretching sheet

$$\sqrt{2}exp\left(\frac{x}{2L}\right)\sqrt{R_e}C_f=\left(1+\frac{1}{\beta}\right)f''(0). \tag{21}$$

Another physical quantity of interest is the local Nusselt number Nu_x, which is defined as

$$Nu_x=\frac{Lq_w}{\kappa(T_w-T_\infty)}\quad \text{where } q_w=-\kappa\left.\frac{\partial T}{\partial y}\right|_{y=0} \tag{22}$$

q_w is known as heat flux from the sheet

$$\frac{Nu_xexp\left(\frac{x}{2L}\right)}{\sqrt{R_e}}=-\theta'(0). \tag{23}$$

Here local Reynold number $R_e=\frac{U_oL}{\vartheta}$.

3. Approximate solution (homotopy analysis method)

Nonlinear differential equations are usually arising from mathematical modeling of many physical systems. Many of them have been solved using numerical methods and some by using analytic methods such as perturbation techniques, Adomian Decomposition and δ-expansion method. Generally speaking, it is still difficult to obtain analytical solutions of nonlinear problems. Aluko and Animasaun [38] adopted the Adomian Decomposition method to obtain semi analytic solution of typical dimensionless momentum and energy equation. It is observed that ADM provides a semi analytic solution which converges within a small domain of independent variable (η). In this research,

the Homotopy analysis method is considered as a method of solution because of its efficiency as an approximate solution of linear and nonlinear differential equations and also, HAM is valid for strongly nonlinear problems even if a given nonlinear problem does not contain any small/large parameters. HAM provides us with a convenient way to adjust the convergence region and rate of approximation series and HAM also provides us with freedom to use different base functions to approximate a nonlinear problem. Introduction to Homotopy theory was introduced by Hilton [39] and the Homotopy Analysis Method (HAM) proposed by Liao [40] to gain analytic approximations of highly nonlinear differential equation. The HAM has some advantages over other traditional analytic approximation methods. First, unlike perturbation techniques, HAM is independent of small/large physical parameters, and thus is valid in more general cases. Besides, different from all other analytic techniques, HAM provides us a convenient way to guarantee the convergence of a series solution. Furthermore, the HAM provides extremely large freedom to choose initial guess and equation-type of linear sub-problems. It is found in Liao [41,42] that lots of nonlinear BVPs in science, engineering and finance can be solved conveniently by means of the HAM, no matter whether the interval is finite or not. Let us consider a differential equation

$$N[f(\eta)] = 0 \tag{24}$$

where N is a nonlinear operator, η denotes independent variable and $f(\eta)$ is an approximate solution of (24) which is an unknown function. Let $f_o(\eta)$ denote an initial approximation of $f(\eta)$, $H(\eta)$ is known as the auxiliary function and L denotes an auxiliary linear operator with the property

$$L[f(\eta)] = 0 \quad \text{when } f(\eta) = 0. \tag{25}$$

Instead of using the traditional Homotopy

$$H[f(\eta; q); q] = (1 - q)L[f(\eta; q) - f_o(\eta)] + qN[f(t; q)]$$

we considered a nonzero auxiliary parameter $\hbar$ and a nonzero auxiliary function $H(\eta)$ to construct a new kind of Homotopy (26) which is more general than traditional Homotopy and a special case when $\hbar = -1$ and $H(\eta) = 1$

$$H[f(\eta); q, \hbar, H(\eta)] = (1 - q)L[f(\eta; q, \hbar, H(\eta)) - f_o(\eta)] - q\hbar H(\eta)N[f(\eta; q, \hbar, H(\eta))] \tag{26}$$

$q \in [0, 1]$ is an embedding parameter and $f(\eta, q)$ is a function of η and q.

When $q = 0$, Eq. (26) becomes

$$H[f(\eta); 0, \hbar, H(\eta)] = L[f(\eta; 0, \hbar, H(\eta)) - f_o(\eta)]. \tag{27}$$

Next step is to find a solution of $H[f(\eta), 0, \hbar, H(\eta)] = 0$. Making use of (25), RHS of Eq. (27) becomes

$$f(\eta; 0, \hbar, H(\eta)) = f_o(\eta). \tag{28}$$

Eq. (28) is the solution of $H[f(\eta), 0, \hbar, H(\eta)] = 0$. When $q = 1$, Eq. (26) becomes

$$H[f(\eta); 1, \hbar, H(\eta)] = -\hbar H(\eta)N[f(\eta; 1, \hbar, H(\eta))] \tag{29}$$

Considering the solution of $H[f(\eta); 1, \hbar, H(\eta)] = 0$

$$-\hbar H(\eta)N[f(\eta; 1, \hbar, H(\eta))] = 0$$
$$N[f(\eta; 1, \hbar, H(\eta))] = 0 \quad \text{but } \hbar H(\eta) \neq 0.$$

Equating to Eq. (24)

$$N[f(\eta; 1, \hbar, H(\eta))] = N[f(\eta)]..$$

Algebraically,

$$f(\eta; 1, \hbar, H(\eta)) = f(\eta). \tag{30}$$

In many cases, by means of analyzing the physical background and the initial/boundary conditions of the nonlinear differential problem; it is possible to know base functions which are proper to represent the solution, even without

solving the given nonlinear problem. In view of the boundary conditions (19) and (20), $f(\eta)$ and $\theta(\eta)$ can be expressed by the set of base functions of the form

$$\langle \eta^j exp(-nj) \mid j \geq 0, n \geq 0 \rangle. \tag{31}$$

The solutions [$f(\eta)$ and $\theta(\eta)$] can be represented in a series form as

$$f(\eta) = a_{0,0}^0 + \sum_{n=0}^{\infty} \sum_{k=0}^{\infty} a_{n,k}^k \eta^k exp(-nj) \tag{32}$$

$$\theta(\eta) = \sum_{n=0}^{\infty} \sum_{k=0}^{\infty} b_{n,k}^k \eta^k exp(-nj), \tag{33}$$

in which $a_{n,k}^k$ and $b_{n,k}^k$ are the coefficients. As long as such a set of base functions is determined, the auxiliary function $H(\eta)$, initial approximations $f_o(\eta)$, $\theta_o(\eta)$ and auxiliary linear operators L_f, L_θ must be chosen in such a way that all solutions of the corresponding high-order deformation of Eqs. (58), (59) exist and can be expressed by this set of base functions. This provides a fundamental rule on how to choose the auxiliary function $H(\eta)$, initial approximations $f_o(\eta)$, $\theta_o(\eta)$ and auxiliary linear operators L_f, L_θ called *rule of solution expression*. This rule plays an important role in the frame of the Homotopy analysis method, as shown in this research. As mentioned above, a real function $f(x)$ might be expressed by many different base functions. Thus, their might exist some different kinds of rule of solution expressions and all of them might give accurate approximations for a given nonlinear problem. In this case we might gain the best one by choosing the best set of base functions. The auxiliary linear operator L, initial approximations $f_o(\eta)$, $\theta_o(\eta)$ and auxiliary function $H(\eta)$ are useful to construct the zero-order deformation equation. Invoking the rule of solution expressions above for $f(\eta)$ and $\theta(\eta)$ on (17), (18) together with boundary conditions (19)–(20), the initial guesses $f_o(\eta)$ and $\theta_o(\eta)$ which satisfy both the initial and boundary conditions (19), (20) are

$$f_o(\eta) = 1 + S - exp(-\eta) \qquad \theta_o(\eta) = exp(-\eta). \tag{34}$$

Linear operators L_f and L_θ are

$$L_f[f(\eta; q)] = \frac{\partial^3 f(\eta; q)}{\partial \eta^3} - \frac{\partial f(\eta; q)}{\partial \eta} \tag{35}$$

$$L_\theta[\theta(\eta; q)] = \frac{\partial^2 \theta(\eta; q)}{\partial \eta^2} - \theta(\eta; q). \tag{36}$$

The operators L_f and L_θ have the following properties

$$L_f[C_1 + C_2 exp(-\eta) + C_3 exp(\eta)] = 0 \qquad L_\theta[C_4 exp(-\eta) + C_5] = 0, \tag{37}$$

in which C_1, C_2, C_3, C_4 and C_5 are constants.

3.1. Zero order of deformation

Let $q \epsilon [0, 1]$ denote the embedding parameter, $\hbar_f$ and $\hbar_\theta$ are non-zero auxiliary parameters. The zero order deformation equation ($m = 0$) is of the form

$$(1 - q)L_f[f(\eta; q) - f_o(\eta)] = q\, \hbar_f\, H_f(\eta) N[f(\eta; q), \theta(\eta; q)] \tag{38}$$

$$(1 - q)L_\theta[\theta(\eta; q) - \theta_o(\eta)] = q\, \hbar_\theta\, H_\theta(\eta) N[f(\eta; q), \theta(\eta; q)]. \tag{39}$$

Subject to boundary conditions

$$f(\eta = 0; q) = S, \qquad \frac{\partial f(\eta = 0; q)}{\partial \eta}, \qquad \theta(\eta = 0; q) = 1 \tag{40}$$

$$\frac{\partial f(\eta \to \infty; q)}{\partial \eta}, \qquad \theta(\eta \to \infty; q) = 0 \tag{41}$$

where the nonlinear operators are defined as

$$\left(1+\frac{1}{\beta}\right)[1+\xi-\theta(\eta;q)\xi]\frac{\partial^3 f(\eta;q)}{\partial\eta^3}-\xi\left(1+\frac{1}{\beta}\right)\frac{\partial\theta(\eta;q)}{\partial\eta}\frac{\partial^2 f(\eta;q)}{\partial\eta^2}-2\left(\frac{\partial f(\eta;q)}{\partial\eta}\right)^2 + f(\eta;q)\frac{\partial^2 f(\eta;q)}{\partial\eta^2}-H_a\frac{\partial f(\eta;q)}{\partial\eta}+J_T\theta(\eta;q)\xi=0 \tag{42}$$

$$\left[1+\frac{4}{3N}+\theta(\eta;q)\varepsilon\right]\frac{\partial^2\theta(\eta;q)}{\partial\eta^2}+\varepsilon\left(\frac{\partial\theta(\eta;q)}{\partial\eta}\right)^2-P_r\theta(\eta;q)\frac{\partial f(\eta;q)}{\partial\eta} + P_r f(\eta;q)\frac{\partial\theta(\eta;q)}{\partial\eta}+P_r\gamma exp(-n\eta)=0. \tag{43}$$

When $q=0$, zero order of deformation Eqs. (38)–(39) leads to

$$L_f[f(\eta;0)-f_o(\eta)]=0, \qquad L_\theta[\theta(\eta;0)-\theta_o(\eta)]=0.$$

With the property

$$f(\eta;0)=f_o(\eta) \tag{44}$$
$$\theta(\eta;0)=\theta_o(\eta), \tag{45}$$

subject to

$$f(\eta=0;0)=S, \qquad \frac{\partial f(\eta=0;0)}{\partial\eta}, \qquad \theta(\eta=0;0)=1 \tag{46}$$

$$\frac{\partial f(\eta\to\infty;0)}{\partial\eta}, \qquad \theta(\eta\to\infty;0)=0. \tag{47}$$

When $q=1$, zero order of deformation Eqs. (38)–(39) leads to

$$0=\hbar_f H_f(\eta)N[f(\eta;1),\theta(\eta;1)], \qquad 0=\hbar_\theta H_\theta(\eta)N[f(\eta;1),\theta(\eta;1)].$$

Based on the fact that $\hbar_f H_f(\eta)\neq 0$ and $\hbar_\theta H_\theta\neq 0$ but

$$0=N[f(\eta;1),\theta(\eta;1)] \tag{48}$$
$$0=N[f(\eta;1),\theta(\eta;1)]. \tag{49}$$

Equating (48) and (49) with (24), we have

$$f(\eta;1)=f(\eta) \tag{50}$$
$$\theta(\eta;1)=\theta(\eta), \tag{51}$$

subject to

$$f(\eta=0;1)=S, \qquad \frac{\partial f(\eta=0;1)}{\partial\eta}, \qquad \theta(\eta=0;1)=1 \tag{52}$$

$$\frac{\partial f(\eta\to\infty;1)}{\partial\eta}, \qquad \theta(\eta\to\infty;1)=0. \tag{53}$$

3.2. High order of deformation

Expanding $f(\eta;q)$ and $\theta(\eta;q)$ in Taylor series with respect to the embedding parameter q,

$$f(\eta;q)=f_o(\eta)+\sum_{m=1}^{\infty}f_m(\eta)q^m \quad \text{where } f_m(\eta)=\frac{1}{m!}\frac{\partial^m f(\eta;q)}{\partial\eta^m}\bigg|_{q=0} \tag{54}$$

$$\theta(\eta;q)=\theta_o(\eta)+\sum_{m=1}^{\infty}\theta_m(\eta)q^m \quad \text{where } \theta_m(\eta)=\frac{1}{m!}\frac{\partial^m\theta(\eta;q)}{\partial\eta^m}\bigg|_{q=0}. \tag{55}$$

Since we are sure that the series (54) and (55) converge at $q = 1$, we have

$$f(\eta; q) = f_o(\eta) + \sum_{m=1}^{\infty} f_m(\eta) q^m \tag{56}$$

$$\theta(\eta; q) = \theta_o(\eta) + \sum_{m=1}^{\infty} \theta_m(\eta) q^m. \tag{57}$$

For the mth order deformation, differentiate (38)–(39) m times with respect to q, divide by $m!$ and set $q = 0$, then we have

$$L_f[f_m(\eta) - \chi_m f_{m-1}(\eta)] = \hbar_f \, H_f(\eta) R_m^f(\eta) \tag{58}$$

$$L_\theta[\theta_m(\eta) - \chi_m \theta_{m-1}(\eta)] = \hbar_\theta \, H_\theta(\eta) R_m^\theta(\eta), \tag{59}$$

subject to

$$f_m(\eta = 0) = 0, \qquad \frac{df_m(\eta = 0)}{d\eta} = 0, \qquad \theta_m(\eta = 0) = 0 \tag{60}$$

$$\frac{df_m(\eta \to \infty)}{d\eta} \to 0, \qquad \theta_m(\eta \to \infty) \to 0 \tag{61}$$

where

$$\begin{aligned} R_m^f(\eta) \; = \; & \left(1 + \frac{1}{\beta}\right)[1 + \xi]\frac{d^3 f_{m-1}}{d\eta^3} - \xi \sum_{k=0}^{m-1} \theta_{m-1-k} \frac{d^3 f_k}{d\eta^3} \\ & - \xi \left(1 + \frac{1}{\beta}\right) \sum_{k=0}^{m-1} \frac{\theta_{m-1}}{d\eta} \frac{d^2 f_{m-1-k}}{d\eta^2} - 2 \sum_{k=0}^{m-1} \frac{df_{m-1-k}}{d\eta} \frac{df_k}{d\eta} \\ & + \sum_{k=0}^{m-1} f_{m-1-k} \frac{d^2 f_k}{d\eta^2} - H_a \frac{df_{m-1}}{d\eta} + J_T \theta_{m-1} \xi \end{aligned} \tag{62}$$

$$\begin{aligned} R_m^\theta(\eta) \; = \; & \left[1 + \frac{4}{3N}\right] \frac{d^2\theta_{m-1}}{d\eta^2} + \varepsilon \sum_{k=0}^{m-1} \theta_m \frac{d^2\theta_{m-1-k}}{d\eta^2} + \varepsilon \sum_{k=0}^{m-1} \frac{d\theta_{m-1-k}}{d\eta} \frac{d\theta_k}{d\eta} \\ & - P_r \sum_{k=0}^{m-1} \theta_k \frac{df_{m-1-k}}{d\eta} + P_r \sum_{k=0}^{m-1} f_k \frac{d_{m-1-k}}{d\eta} + P_r \gamma exp(-n\eta) \end{aligned} \tag{63}$$

and

$$\begin{aligned} \chi_m &= 0 \quad \text{when } m \leq 1 \\ \chi_m &= 1 \quad \text{when } m > 1. \end{aligned} \tag{64}$$

According to the rule of solution expression, the rule of coefficient ergodicity and the rule of solution existence as discussed by Liao [41] we choose auxiliary functions as

$$H_f = H_\theta = 1. \tag{65}$$

4. Convergence of homotopy solution

Liao [41] revealed that whenever an approximate solution converges, it will be one of the solutions of considered problem. Therefore, it is important to ensure that the solutions series are convergent. It is very necessary to prove the convergence of the solution series, the convergence and rate of approximation for the HAM solution of the series which are strongly dependent upon the auxiliary parameter. Therefore, one can choose the proper values of $\hbar_f$ and $\hbar_\theta$ by plotting the $\hbar$-curves which ensure that the solution series (54) and (55) converge as suggested by

Table 1
Comparison of $-\theta'(0)$ at 10th-order approximation for several values of Prandtl number with Nazar and Bidin [9].

P_r	$K = 0.5$ Nazar and Bidin [43]	$N = 2$ in present
1	0.6765	0.676506980749169
2	1.0735	1.073521347405536
3	1.3807	1.380754270594433
P_r	$K = 1$ Nazar and Bidin [43]	$N = 1$ in present
1	0.5315	0.531241548130990
2	0.8627	0.862772689888035
3	1.1214	1.121429576505715

[41,42]. In the present work, the optimal homotopy analysis approach [42] is used to obtain the optimal values of the auxiliary parameters by means of the minimum of the residual squares of the governing equations. Using the symbolic computation software Wolfram Mathematica, we directly employed the command "Minimize" to get the optimal convergence-control parameter. In order to validate the accuracy of our approximate solution (Homotopy Analysis Method) and to examine the application of the program applied, we have compared our results at 10th order of approximation with heat transfer coefficients $-\theta'(0)$ $[E = 0]$ of Bidin and Nazar [43] when $\beta = \infty$, $H_a = \xi = J_T = \varepsilon = \gamma = S = 0$. It is very important to note that $k = 0.5$ in [43] is equivalent to $N = 2$ in the present study. The results are found in excellent agreement and some of the comparisons are shown in Table 1.

The interval on $\hbar$-axis for which the $\hbar$-curve becomes parallel to the $\hbar$-axis is recognized as the set of admissible values of $\hbar_f$ and $\hbar_\theta$ for which the solution series converges. For this purpose the $\hbar$-curves are plotted for 10th-order of approximations in Figs. 2 and 3 using $\beta = 0.2$, $\xi = 1$, $J_T = 1$, $H_a = 0.2$, $\varepsilon = 0.3$, $N = 0.7$, $P_r = 0.72$, $\gamma = 0.5$, $n = 0.5$, $S = 0.3$. These figures show that the ranges for the acceptable values of $\hbar_f$ and $\hbar_\theta$ are $-0.20 \leq \hbar_f \leq -0.17$ and $-0.15 \leq \hbar_\theta \leq -0.4$. Obviously from the $\hbar$-curves for this problem, we obtained the approximate optimal values of $\hbar_f$ and $\hbar_\theta$ at 10th order of approximation as -0.16920296515000335 and -0.2728946683726691 respectively. At these optimal values, $f''(0) = -0.4699738574392338$ and $\theta'(0) = -0.39372718040951327$.

5. Results and discussion

In order to analyze the approximate solutions, computation has been carried out using the method described in the previous section for various values of temperature dependent plastic dynamic variable viscosity parameter (ξ), non-Newtonian Casson parameter (β), local modified Grashof related parameter (J_T), temperature dependent variable thermal conductivity parameter (ε), thermal radiation parameter (N), Prandtl number (P_r), space dependent internal heat source parameter (γ) and intensity of internal heat generation parameter on space (n). For graphical illustrations of the results, see Figs. 4–19. Fig. 4 illustrates the velocity profiles for different values of temperature dependent plastic dynamic viscosity parameter (ξ) when the magnitude of magnetic field is high (i.e. $H_a = 1.2$) and in the presence of suction (i.e. $S = 0.3$). It is observed that when Casson fluid is treated as fluid with constant plastic dynamic viscosity throughout the boundary layer, the velocity is found to be very small in quantity throughout the boundary layer compared to when treated as variable plastic dynamic viscosity. This figure demonstrates the effect of increasing ξ (i.e. to increase the resulting temperature of $(T_w - T_\infty)$ at constant value of b which makes the bond between Casson fluids to become weaker and drastically decreases the strength of plastic dynamic viscosity). This effect eventually increases the transport phenomena across the momentum boundary layer. In Fig. 5, variations of temperature field $\theta(\eta)$ against η for several values of (ξ) using $P_r = 0.72$, $\gamma = 4$ and $n = 0.5$ are shown. The figure depicts the strong effect of the intensity of internal heat generation across the space. It is observed that the temperature decreases as $\eta \to 8$. Increase in the magnitude of temperature dependent plastic dynamic viscosity parameter leads to decrease in thermal boundary layer thickness, which results in decrease of temperature profile $\theta(\eta)$. As the fluid temperature increases (i.e. ξ increases), it tries to expand, since the fluid is incompressible, the pressure decreases as its molecules become weak. Hence the fluid consumed all the temperature; this may account for decrease in the temperature. Decrease in temperature profiles across the thermal boundary layer means a decrease in the velocity of the Casson fluid. As a matter of fact, in this case, the fluid particles undergo two opposite forces which are: (i)

one force increases the fluid velocity due to decrease in the fluid viscosity with increase in the values of ξ, (ii) the second force decreases the fluid velocity due to decrease in temperature; since $\theta(\eta)$ decreases with increasing ξ. Very near the vertical surface, as the temperature $\theta(\eta)$ is high, the first force dominates and far away from the surface, the temperature $\theta(\eta)$ is low; this implies that the second force dominates in that region. Fig. 6 represents the velocity profiles for the variation of magnetic field parameter H_a when $\xi = 1$. The velocity decreases significantly throughout the fluid domain.

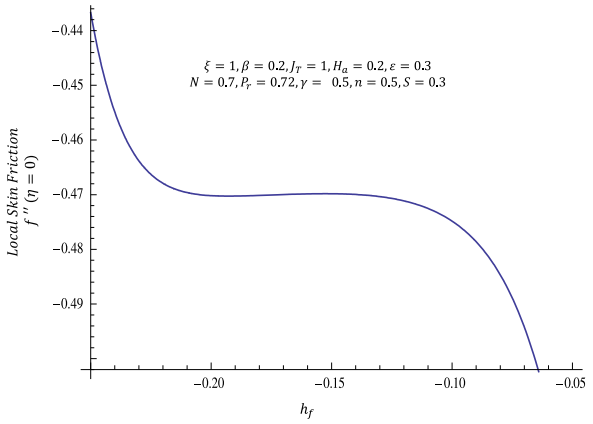

Fig. 2. The $\hbar_f$-curve of $f''(0)$ obtained at 10th-order approximation.

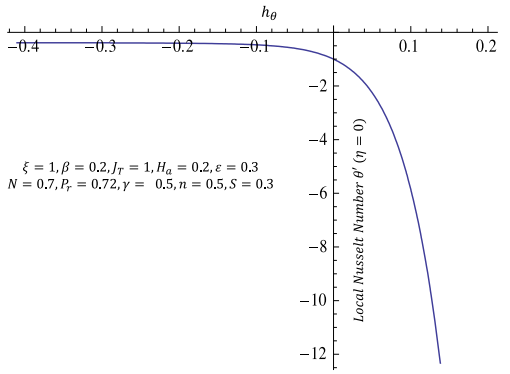

Fig. 3. The $\hbar_\theta$-curve of $\theta'(0)$ obtained 10th-order approximation.

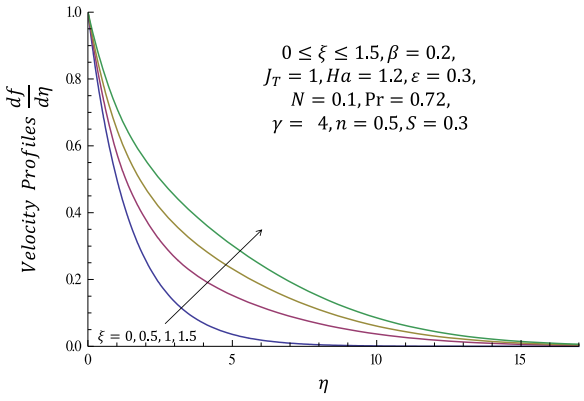

Fig. 4. Effect of temperature dependent variable plastic dynamic viscosity parameter over velocity profiles.

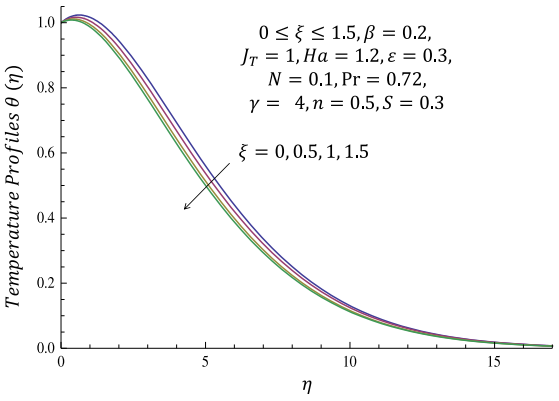

Fig. 5. Effect of temperature dependent variable plastic dynamic viscosity parameter over temperature profiles.

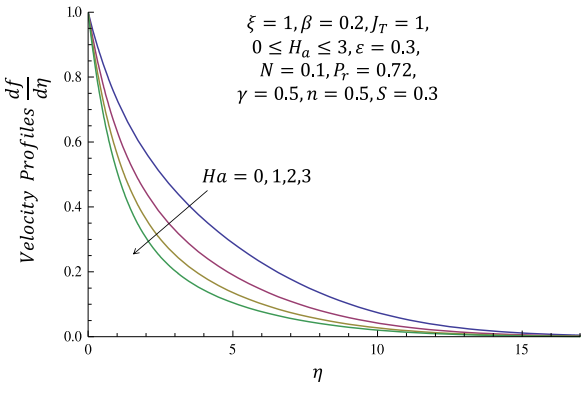

Fig. 6. Effect of magnetic field parameter over velocity profiles.

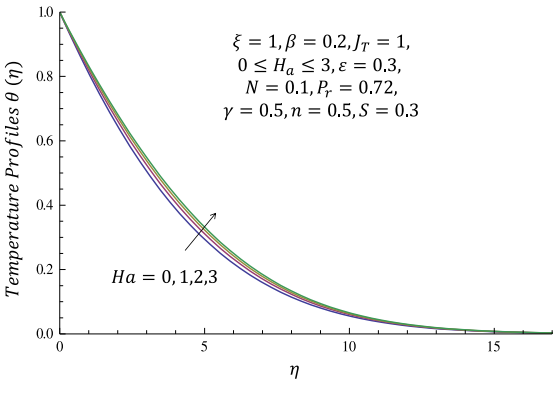

Fig. 7. Effect of magnetic field parameter over temperature profiles.

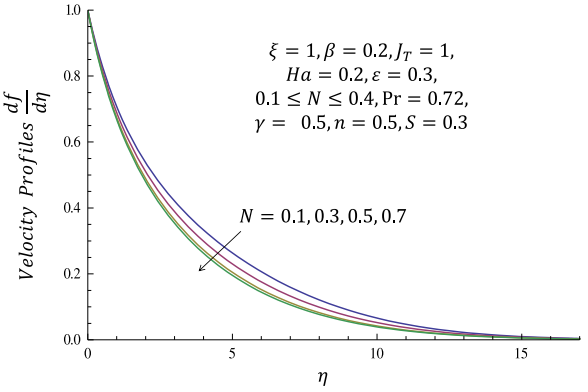

Fig. 8. Effect of thermal radiation parameter over velocity profiles.

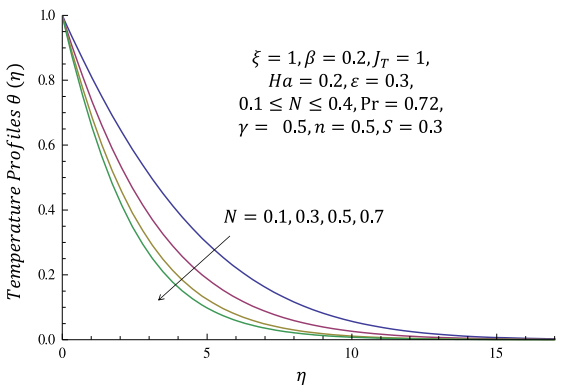

Fig. 9. Effect of thermal radiation parameter over temperature profiles.

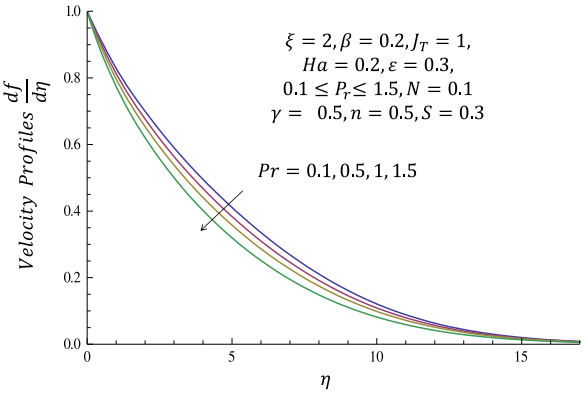

Fig. 10. Effect of Prandtl number over velocity profiles.

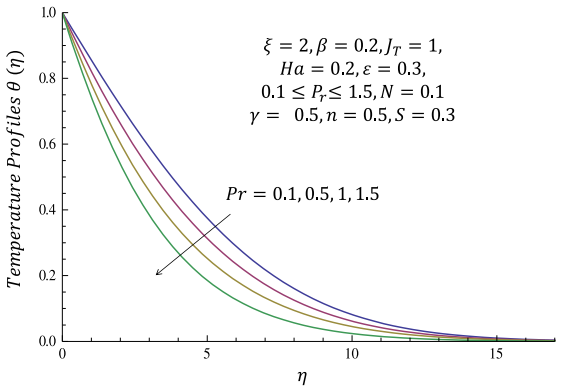

Fig. 11. Effect of Prandtl number over temperature profiles.

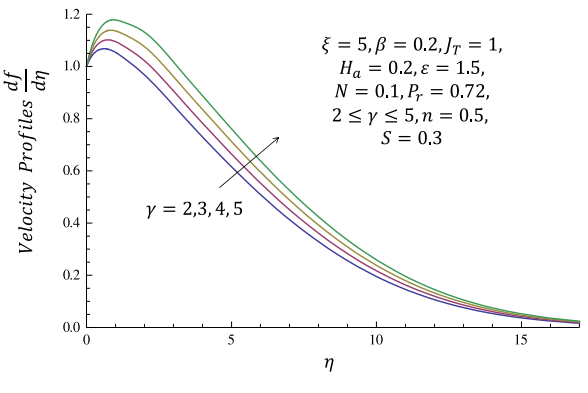

Fig. 12. Effect of space dependent internal heat source parameter over temperature profiles.

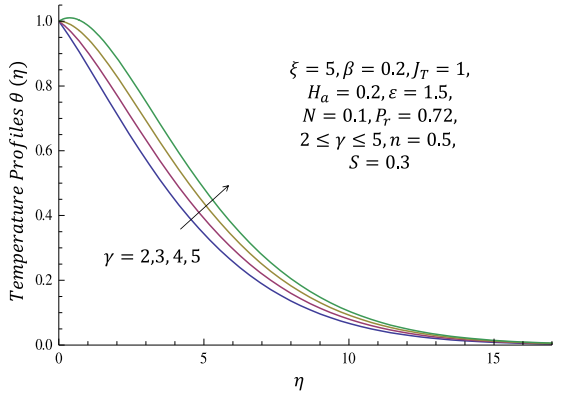

Fig. 13. Effect of space dependent internal heat source parameter over temperature profiles.

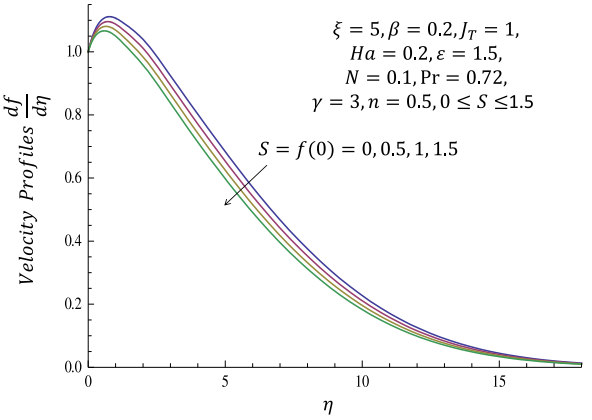

Fig. 14. Effect of suction parameter over temperature profiles.

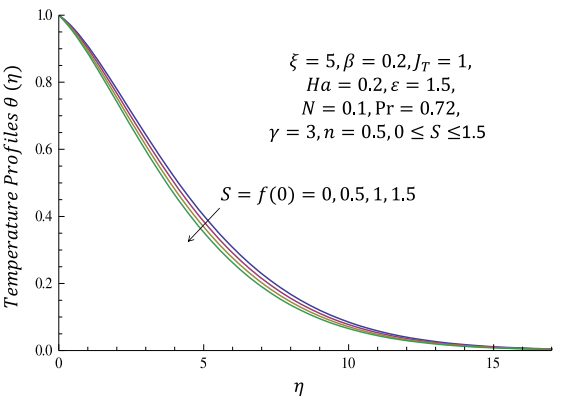

Fig. 15. Effect of suction parameter over temperature profiles.

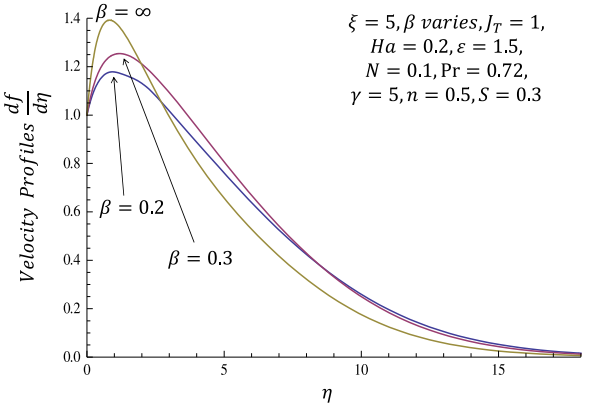

Fig. 16. Effect of Casson fluid parameter over velocity profiles.

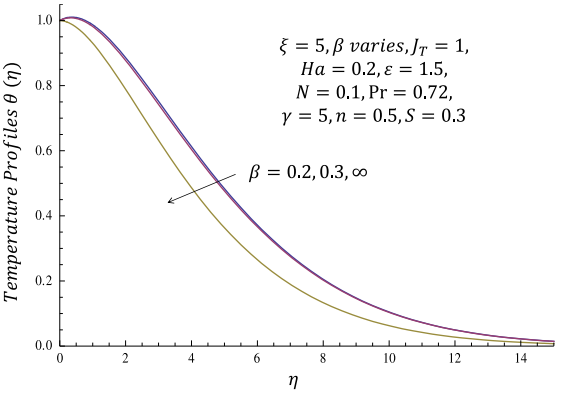

Fig. 17. Effect of Casson fluid parameter over temperature profiles.

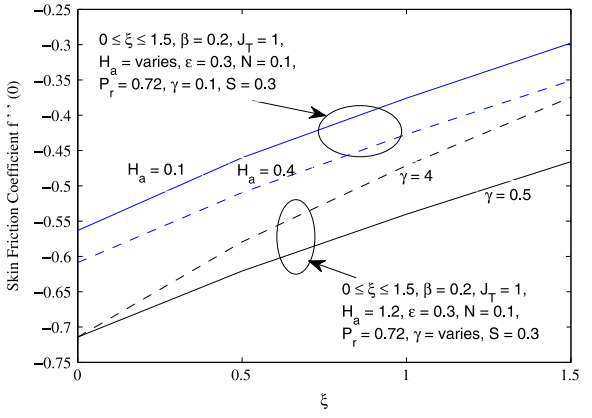

Fig. 18. Skin friction coefficient $f''(0)$ against temperature dependent variable fluid viscosity parameter ξ at various values of Ha and γ.

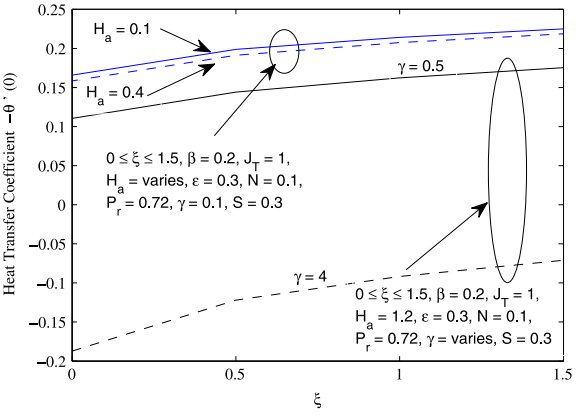

Fig. 19. Heat transfer coefficient $-\theta'(0)$ against temperature dependent variable fluid viscosity parameter ξ at various values of Ha and γ.

Application of a magnetic field to an electrically conducting Casson fluid produces a kind of drag-like force called Lorentz force. This force causes reduction in the fluid velocity within boundary layer. It is observed that as Ha increases, the temperature distribution increases. The effect of Lorentz force on velocity profiles generated a kind of friction on the flow; this friction in turn generated more heat energy which eventually increases the temperature distribution in the flow (see Fig. 7). Effect of radiation parameter N on the momentum boundary layer and thermal boundary layer is shown in Figs. 8 and 9 respectively using $\xi = 1$, $P_r = 0.72$, $\gamma = 0.5$ and $n = 0.5$. For different values of the radiation parameter N, it is noticed that an increase in the radiation parameter results in a decrease in the velocity and temperature within the boundary layer. The effect of radiation parameter N is to reduce the temperature significantly in the flow region. The increase in radiation parameter means the release (i.e. channel to loss) heat energy from the flow region and so the fluid temperature decreases as the thermal boundary layer thickness becomes thinner. Salem and Fathy [37] reported similar trend of velocity and temperature profiles in their study on effect of thermal radiation on MHD convective heat transfer adjacent to a vertical continuously stretching sheet in the presence of variable viscosity. The reason for this trend can be further explained as follows: the effect of radiation is to decrease the rate of energy transport to the fluid, thereby decreasing the temperature of the fluid. From these figures, we also observe that the effect of radiation becomes more significant as $N \to 0$ ($N \neq 0$) and can be neglected when $N \to \infty$. In addition, radiation demonstrates a more pronounced influence on the velocity and the temperature distributions for a fluid with a small P_r ($P_r < 1$, gases) than for one with a large P_r ($P_r > 1$, liquids). Fig. 10 depicts effect of Prandtl number over velocity profiles. As the magnitude of P_r increases, velocity profiles decrease significantly. At a fixed value of specific heat capacity Cp and thermal conductivity κ, increase in the value of Prandtl number $P_r = \frac{Cp\mu}{\kappa}$ simply implies, increase in the magnitude of fluid viscosity.

When the value of fluid viscosity is high this corresponds to fluid with low velocity. In Fig. 11, it is observed that an increase in Prandtl number results in decrease of temperature and thermal boundary layer thickness and in general lower average temperature within the boundary layer. The reason is that smaller values of P_r are equivalent to increasing the thermal conductivities, and therefore heat is able to diffuse away from the heated plate more rapidly than for higher values of P_r. Figs. 12 and 13 exhibit velocity profiles for different values of exponentially decaying internal heat generation parameter when $\xi = 5$ and $\beta = 0.2$. The velocity profile and temperature profile increase as γ ranges within $2 \leq \gamma \leq 5$. Fig. 14 presents the effect of suction on fluid velocity when the temperature dependent fluid viscosity is uniform (i.e. $\xi = 5$), with increase in the magnitude suction parameter when $N = 0.1$, $P_r = 0.72$, the velocity is found to decrease (i.e. suction causes decrease of the fluid velocity in the momentum boundary layer region). The physical explanation for such a behavior is as follows: (i) In case of suction, the heated fluid is pushed towards the wall where the buoyancy forces can act to retard the fluid due to high influence of the viscosity, (ii) this effect acts to decrease the wall shear stress and (iii) local Skin friction decreases. Fig. 15 exhibits the temperature $\theta(\eta)$ with the increasing suction parameter S. The thermal boundary layer thickness decreases with an increase in the value of suction parameter; this causes an increase in the rate of heat and mass transfer. The explanation for such behavior is that the fluid is brought closer to the surface and reduces the thermal boundary layer thickness in case of suction. As such, then the presence of wall suction decreases velocity boundary layer thickness. Figs. 16 and 17 depict the effect of non-Newtonian Casson fluid parameter over velocity and temperature profiles.

Casson fluid is treated as fluid with variable plastic dynamic viscosity (i.e. $\xi = 5$) with strong effect of yield stress P_y, the velocity increases near the wall ($0 \leq \eta \leq 7.2$) and negligibly decreases far from the vertical heated wall when β increases within $0.2 \leq \beta \leq 0.3$. It is further observed that, as the nature of the fluid is tending towards the nature of Newtonian fluid (i.e. $\beta \to \infty$), the velocity increases greatly within a layer of fluids near the vertical wall. The result is obvious for this case when $\xi = 5$ means temperature has been injected into the non-Newtonian fluid. More heat is injected into the fluid layers since temperature of the exponentially stretching surface $\theta(\eta = 0) = 1$ and, hence the intermolecular forces within plastic dynamic viscosity is broken greatly near the wall ($\eta = 0$) where the heat can be felt. This account for increase in the velocity profiles near the wall and decrease in temperature profiles. Figs. 18 and 19 exhibit the nature of skin-friction coefficient $f''(0)$ and heat transfer coefficient $-\theta'(0)$ with temperature dependent variable fluid viscosity parameter ξ for two values of magnetic field parameter ($H_a = 0.1, 0.4$) and also for two values of space dependent internal heat source parameter ($\gamma = 0.5, 4$) respectively. It is found that skin-friction coefficient $f''(0)$ increases with increase in ξ and decreases with increase in H_a. It is further observed that $f''(0)$ increases with increase in ξ and also increases with increase in γ. In Fig. 19, heat transfer coefficient $-\theta'(0)$ increases with increase in ξ and decreases with increase in H_a. In the same figure, heat transfer coefficient increases with increase

Table 2
Variation of $f''(0)$ and $-\theta'(0)$ at 10th-order approximation when $\xi = \varepsilon = \gamma = 0$, $\beta = 0.2$, $J_T = 1$, $N = 0.1$, $P_r = 0.72$, $S = 0.3$ and $H_a = varies$.

H_a	$f''(0)$	$-\theta'(0)$
0.4	−0.608590715730847	0.169675636346164
0.6	−0.636817665101602	0.165530795062700
0.8	−0.663735097058842	0.161849230188970

in ξ and decreases with increase in γ. When Casson fluid is treated as fluid with constant thermo-physical property in the absence of exponentially heat source as shown in Table 2, it is observed that $f''(0)$ which is related to skin friction coefficient decreases significantly while $-\theta(0)$ which is related to local heat transfer decreases negligible as magnitude of H_a increases. The significant decrease in the corresponding value of $f''(0)$ can be traced to the retardation of velocity profiles owing to increase in Lorentz force with an increase in magnetic field parameter.

6. Concluding remarks

Laminar free convective MHD boundary layer flow of non-Newtonian Casson fluid flow over an exponentially stretching surface embedded in a thermally stratified medium has been studied. An approximate solution (HAM) approach was utilized to study the effect of all the controlling parameters on the flow's velocity and temperature profiles in the boundary layer. The results reveal that:

- An increase in the variable plastic dynamic viscosity parameter of Casson fluid corresponds to an increase in the velocity profiles and a decrease in temperature throughout the boundary layer.
- Based on the results of the present study, it can be concluded that the effect of Casson fluid parameter when treated as fluid with variable plastic dynamic viscosity, the velocity profile increases, temperature distribution decreases.
- Variation of exponentially decaying heat source parameter shows significant effect on the thickness of the boundary layer profiles (i.e. velocity and temperature).
- The magnetic field reduces the heat transfer rate, though it causes the increment in the temperature inside the boundary layer.

Acknowledgments

The authors appreciate the constructive comments of the reviewers which led to definite improvement of this study. This research is dedicated to the memory of Late Professor Emmanuel Adewumi Adebile who passed away on 16th October, 2014.

References

[1] Sakiadis BC. Boundary layer behavior on continuous solid surface I-boundary layer equations for two dimensional and axisymmetric flow. AlChE J 1961;7:26–8.
[2] Sakiadis BC. Boundary Layer behavior on continuous solid surface II-Boundary Layer behavior on continuous flat surface. AlChE J 1961;7: 221–35.
[3] Crane LJ. Flow past a stretching plate. Z Angew Math Phys 1970;21:645–7.
[4] Carragher P, Crane LJ. Heat transfer on a continuous stretching sheet. Z Angew Math Mech 1982;62:564–73.
[5] Ibrahim SM. Heat and mass transfer effects on steady MHD flow over an exponentially streatching surface with viscous Dissipation, heat generation and radiation. J Global Res Math Arch 2013;1:8.
[6] Bararnia H, Haghparast N, Miansari Mo, Barari A. Flow analysis for the Falkner–Skan wedge flow. Current Sci 2012;103:169–77.
[7] Elbashbeshy EMA. Heat transfer over an exponentially stretching continuous surface with suction. Arch Mech 2001;53:643–51.
[8] Khan SK, Sanjayanand E. Viscoelastic boundary layer flow and heat transfer over an exponential stretching sheet. Int J Heat Mass Transfer 2005;48:1534–42.
[9] Partha MK, Murthy PVSN, Rajasekhar GP. Effect of viscous dissipation on the mixed convection heat transfer from an exponentially stretching surface. Heat Mass Transf 2005;41:360–6.
[10] Ishak A. MHD boundary layer flow due to an exponentially stretching sheet with radiation effect. Sains Malaysiana 2011;40:391–5.
[11] Bhattacharyya K. Boundary layer flow and heat transfer over an exponentially shrinking sheet. Chin Phys Lett 2011;28:074701. http://dx.doi.org/10.1088/0256-307X/28/7/074701.

[12] Bhattacharyya K, Pop I. MHD boundary layer flow due to an exponentially shrinking sheet. J Magnetohydrodynamics (Salaspils, Lativia) 2011;47:337–44.
[13] Bhattacharyya K, Vajravelu K. Stagnation-point flow and heat transfer over an exponentially shrinking sheet. Commun Nonlinear Sci Numer Simul 2012;17:2728–34.
[14] Casson N. A flow equation for pigment oil-suspensions of the printing ink type. In: Mill CC, editor. Rheology of disperse systems. Pergamon Press; 1959. p. 84.
[15] Rao AS, Prasad VR, Reddy NB, Bég OA. Heat transfer in a Casson rheological fluid from a semi-infinite vertical plate with partial slip. Wiley Periodicals, Inc.; 2013. http://dx.doi.org/10.1002/htj.21115. Heat Trans Asian Res Published online in Wiley Online Library.
[16] Bird RB, Dai GC, Yarusso BJ. The rheology and flow of viscoplastic materials. Rev Chem Eng 1983;1:1–83.
[17] Mitsoulis E. Flows of viscoplastic materials: Models and computations. The British society of rheology. 2007. p. 135–78.
[18] Mukhopadhyay S. Casson fluid flow and heat transfer over a nonlinearly stretching surface. Chin Phys 2013;22:7.
[19] Hayat T, Shehzadi SA, Alsaedi A. Soret and Dufour effects on magnetohydrodynamic (MHD) flow of Casson fluid. Appl Math Mech Engl Ed 2012;33:1301–12. http://dx.doi.org/10.1007/s10483-012-1623-6.
[20] Fredrickson AG. Principles and applications of rheology. NJ, USA: Prentice-Hall Englewood Cliffs; 1964.
[21] Mustafa M, Hayat T, Pop I, Aziz A. Unsteady boundary layer flow of a Casson fluid due to an impulsively started moving flat plate. Heat Transfer 2011;40:563–76. http://dx.doi.org/10.1002/htj.20358.
[22] Animasaun IL. Effects of thermophoresis, variable viscosity and thermal conductivity on free convective heat and mass transfer of non-darcian MHD dissipative Casson fluid flow with suction and *n*th order of chemical reaction. J Nigerian Math Soc 2014; http://dx.doi.org/10.1016/j.jnnms.2014.10.008.
[23] Tasaka Y, Kudoh Y, Takeda Y, Yanagisawa T. Experimental investigation of natural convection induced by internal heat generation. Journal of Physics IOP: Conference Series 2005;14:168–79. http://dx.doi.org/10.1088/1742-6596/14/1/021.
[24] Sahin AZ. Transient heat conduction in semi-infinite solid with spatially decaying exponentially heat generation. Int Commun Heat Mass Transfer 1992;19:349–58.
[25] Crepeau JC, Clarksean R. Similarity solutions of natural convection with internal heat generation. Trans ASME C 1997;119:184–5.
[26] Salem AM, El-Aziz MA. MHD-mixed convection and mass transfer from a vertical stretching sheet with diffusion of chemically reactive species and space- or temperature-dependent heat source. Can J Phys 2007;85:359–73. http://dx.doi.org/10.1139/P07.048.
[27] Salem AM, El-Aziz MA. Effect of Hall currents and chemical reaction on hydromagnetic flow of a stretching vertical surface with internal heat generation/absorption. Appl Math Model 2008;32:1236–54. http://dx.doi.org/10.1016/j.apm.2007.03.008.
[28] Makinde OD. Effect of variable viscosity on thermal boundary Layer over a permeable flat plate with radiation and c Convective surface boundary condition. J Mech Sci Technol 2012;26:5.
[29] Abo-Eldahab EM, Abd El-Aziz M. Blowing/suction effect on hydromagnetic heat transfer by mixed convection from an inclined continuously stretching surface with internal heat generation/absorption. Int J Therm Sci 2004;43:709. 2004.
[30] Chamkha AJ, Khaled AA. Similarity solutions for hydromagnetic simultaneous heat and mass transfer by natural convection from an inclined plate with internal heat generation or absorption. Heat Mass Transfer 2001;37:117.
[31] Salem AM, Fathy R. Effect of thermal radiation on MHD mixed convective heat transfer adjacent to a vertical continuously stretching sheet in the presence of variable viscosity. J Korean Phys Soc 2010;57:6.
[32] Raptis A. Radiation and free convection flow through a Porous medium. Int Commun Heat Mass Transfer 1998;25:289–95.
[33] Sparrow EM, Cess RD. Radiation heat transfer. Washington, DC: Augmented edition Hemisphere Publ. Crop; 1978 [chapters 7 and 10].
[34] Layek GC, Mukhopadhyay S, Samad SkA. Study of MHD boundary layer flow over a heated stretching sheet with variable viscosity. Int J Heat Mass Transfer 2005;48:4460–6.
[35] Animasaun IL, Aluko OB. Analysis on variable fluid viscosity of non-Darcian flow over a moving vertical plate in a porous medium with suction and viscous Dissipation. International Organization of Scientific Research (Journal of Engineering) 2014;04:18–32. http://dx.doi.org/10.9790/3021-04841832.
[36] Salem AM, Fathy R. Effects of variable properties on MHD heat and mass transfer flow near a stagnation point towards a stretching sheet in a porous medium with thermal radiation. Chin Phys B 2012;21:054701. http://dx.doi.org/10.1088/1674-1056/21/5/054701.
[37] Animasaun IL, Oyem AO. Effect of variable viscosity, Dufour, Soret and thermal conductivity on free convective heat and mass transfer of non-Darcian flow past porous flat surface. Amer J Comput Math 2014;4:357–65. http://dx.doi.org/10.4236/ajcm.2014.44030.
[38] Aluko OB, Animasaun IL. Semi-analytic solution of non-linear coupled differential equation using Adomian decomposition. World J Young Res 2013;3:23–30.
[39] Hilton PJ. An introduction to homotopy theory. Cambridge University Press; 1953.
[40] Liao SJ. The proposed homotopy analysis technique for the solution of nonlinear problems [Ph.D. thesis], Shanghai Jiao Tong University; 1992.
[41] Liao SJ. Beyond perturbation: introduction to the homotopy analysis method. Boca Raton, Fla., USA: Chapman and Hall; 2003.
[42] Liao SJ. An optimal homotopy analysis approach for atrongly nonlinear differential equations. Commun Nonlinear Sci Numer Simul 2010; 15:2003–16.
[43] Bidin B, Nazar R. Numerical solution of the boundary layer flow over an exponentially stretching sheet with thermal radiation. Eur J Sci Res 2009;33:4.